Graphene quantum dots in perpendicular magnetic fields

J. Güttinger, C. Stampfer, T. Frey, T. Ihn and K. Ensslin Solid State Physics Laboratory, ETH Zurich, 8093 Zurich, Switzerland

We report transport experiments on graphene quantum dots. We focus on excited state spectra in the near vicinity of the charge neutrality point and signatures of the electron-hole crossover as a function of a perpendicular magnetic field. Coulomb blockade resonances of a 50 nm wide and 80 nm long dot are visible at all gate voltages across the transport gap ranging from hole to electron transport. The magnetic field dependence of more than 40 states as a function of the back gate voltage can be interpreted in terms of the unique evolution of the diamagnetic spectrum of a graphene dot including the formation of the E=0 Landau level, situated in the center of the transport gap, and marking the electron-hole crossover.

PACS numbers: 73.22.-f, 72.80.Rj, 73.21.La, 75.70.Ak

INTRODUCTION

Graphene nanostructures [1, 2, 3, 4, 5, 6, 7, 8, 9, 10, 11] attract increasing attention mainly due to potential applications in high mobility electronics [12, 13] and solid state quantum information processing [14]. In particular, low nuclear spin concentrations expected in graphene promise long spin lifetimes [14, 15, 16, 17] and make graphene quantum dots (QDs) [4, 5, 6, 7, 8] interesting for spin-qubit operations [14]. Moreover, graphene nanostructures may allow to investigate phenomena related to massless Dirac Fermions in confined dimensions [5, 18, 19, 20, 21, 22]. Intensive research has been triggered by the unique electronic properties of graphene [23] including the gapless linear dispersion, and the unique Landau level (LL) spectrum [24, 25]. The search for signatures of graphene-specific properties in quantum dots is of interest in order to understand the addition spectra, the spin states and dynamics of confined graphene quasi-particles. Recent advances in fabricating width-modulated graphene nanoribbons helped to overcome intrinsic difficulties in (i) creating tunneling barriers and (ii) confining electrons in graphene, where transport is dominated by Klein tunneling-related phenomena [26, 27]. Graphene quantum dots have been fabricated and Coulomb blockade [4, 5], quantum confinement [7, 8] and charge detection [6] have been observed.

Here, we show tunneling spectroscopy (i.e. transport) measurements on a fully tunable graphene quantum dot. We present the evolution of a large number of Coulomb resonances near the charge neutrality point in a magnetic field from the low-field regime to the regime of Landau level formation. In particular, we investigate the quantum dot spectrum in the vicinity of the charge neutrality point as a function of a perpendicular magnetic field (B-field). Near the electron-hole crossover we observe a rich excited state spectrum with inelastic cotunneling lines and unconventional features inside the Coulomb diamonds. Some of these features, which are very pronounced at B=0, quickly disappear in a perpendicular magnetic field. Moreover, we find indications of the

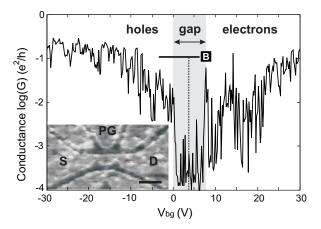


FIG. 1: Low bias $(V_b=100~\mu\mathrm{V})$ back gate characteristic at $V_{pg}=2~\mathrm{V}$. The resolved transport gap (see highlighted region) separates between hole and electron transport. This trace is a back gate cross-section of Fig. 1(e) in Ref. [8], which includes the region [B] marked therein. The dashed line marks the position of the electron-hole crossover identified in Ref. [8]. The inset shows a scanning force microscope image of an etched graphene quantum dot device with source (S) and drain (D) leads and a plunger gate (PG) for electrostatic tunability. The scale bar corresponds to 100 nm.

formation of the lowest (E=0) Landau level at high B-fields marking the electron-hole crossover in graphene devices.

This paper is organized as follows. In section 2 we briefly review the graphene quantum dot device fabrication. Transport measurements at zero magnetic field are discussed in section 3.1. Landau level formation and the magnetic field dependence of inelastic cotunneling processes are addressed in sections 3.2 and 3.3, respectively.

DEVICE FABRICATION

The state-of-the-art fabrication process of graphene nanodevices, which has been mostly developed in Manchester [24, 28], and in New York [25], is based on the

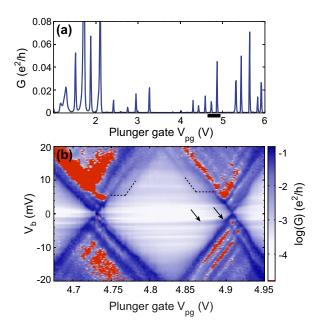


FIG. 2: (color online) (a) Coulomb blockade resonances of the graphene quantum dot as function of plunger gate voltage V_{pg} at $V_{bg} = -0.9$ V. The conductance has been measured at constant bias of $V_b = 100~\mu\text{V}$. (b) Coulomb diamonds, i.e., finite-bias measurement of the quantum dots differential conductance $G_{qd} = dI/dV_b$ as function of V_b and V_{pg} at B = 0. Note the rich excited state spectra and in particular the different vertical distances between the diamond edge and the diagonal structures inside the Coulomb-blockaded region for positive V_b .

mechanical exfoliation of (natural) graphite by adhesive tapes [28]. The substrate material consists of highly doped silicon (Si^{++}) bulk material covered with approximately 300 nm of silicon oxide (SiO_2), where thickness and roughness of the SiO_2 top layer is crucial for the identification and further processing of single-layer graphene samples. Standard photolithography followed by metalization (chrome/gold) and lift-off is used to pattern arrays of reference alignment markers on the substrate that are later used to re-identify locations (of individual graphene flakes) on the chip and to align further processing patterns.

The graphene flake has to be structured to submicron dimensions in order to fulfill the device design requirements (see e.g., figure in the abstract). We use a technique based on resist spin coating, electron beam lithography (EBL), development and subsequent etching of the unprotected graphene. Two successive processing steps have been used including small modifications to decrease the minimum feature size of the graphene nanodevice. First we used a resist [Polymethylmethacrylat (PMMA)] with a thickness of 45 nm and short etching time to define the delicate structures. In the second step a 100 nm thick resist is used for the coarse structuring of the flake also providing a broader process parameter window for the

etching step. It has been found that short (5 and 15 seconds) mainly physical reactive ion etching (RIE) based on argon and oxygen (80/20) provides good results without influencing the overall quality of the graphene flake [29]. After etching and removing the residual EBL resist, the graphene nanostructures are contacted by an additional EBL step, followed by metalization and lift-off. Here we evaporated 2 nm chrome (Cr) and 40 nm gold (Au) for contacting the graphene quantum dot device.

A scanning force microscope image of the device studied here is shown as an inset in Fig. 1. The 50 nm wide and 80 nm long graphene quantum dot is connected to source (S) and drain (D) via two graphene constrictions with a width of 25 nm, both acting as tunneling barriers. The dot and the leads can be further tuned by the highly doped silicon substrate used as a back gate (BG) and an in-plane graphene plunger gate (PG).

MEASUREMENTS

All measurements have been performed in a dilution refrigerator at a base temperature of $T\approx 90$ mK. We have measured the two-terminal conductance through the graphene quantum dot device by applying a symmetric DC bias voltage V_b while measuring the current through the quantum dot device with a noise level below 10 fA. For differential conductance measurements a small AC bias, $V_{b,ac}=40~\mu\mathrm{V}$ has been superimposed on V_b and the differential conductance has been measured with lock-in techniques at a frequency of 18.9 Hz.

In Fig. 1 we show the differential conductance as a function of back gate voltage at low bias ($V_b = 100~\mu V$) highlighting the strong suppression of the conductance around the charge neutrality point ($0 < V_{bg} < 7.5~V$) due to the so-called transport gap [30, 31]. Here we tune transport from the deep hole to the deep electron regime, as illustrated in Fig. 1. The large number of resonances within the gap region may be due to both, (i) resonances in the graphene constrictions acting as tunneling barriers [4] (and thus being main responsible for the large extension of this transport gap) and (ii) Coulomb resonances of the quantum dot itself.

Coulomb blockade measurements at B=0

By fixing the back gate voltage at a value close to the transport gap (e.g., $V_{bg} = -0.9 \text{ V}$) and sweeping the lateral plunger gate voltage (V_{pg}) in a narrow range close to the charge neutrality point (see below) Coulomb blockade resonances of the graphene quantum dot can be well resolved, as shown in Fig. 2(a). The strong amplitude modulation of the conductance peaks [see e.g., on the very left of Fig. 2(a)] is mainly due to transparency modulations of the constrictions [4], which can dominate

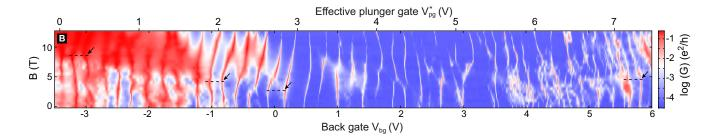


FIG. 3: Evolution of Coulomb blockade resonances in perpendicular magnetic field. The conductance is plotted as function of back gate voltage V_{bg} and magnetic field B ($V_b = 500 \ \mu\text{V}$). The effective plunger gate voltage V_{pg}^* , calculated via the relative lever arm, is given on the top of the graph. This data have been measured in the regime marked by the solid line [B] in Fig. 1(e) of Ref. [8].

the width of the Coulomb resonances and significantly elevate the conductance. In Fig. 2(b) we show corresponding Coulomb diamond measurements [see black bar in Fig. 2(a), that are measurements of the differential conductance $(G = dI/dV_b)$ as a function of bias voltage V_b and plunger gate voltage V_{pg} . Note, that this measurement was recorded at a higher base temperature of T = 370 mK. The reason for this slightly higher temperature is the good visibility of the diagonal lines inside the diamond. The overall structure of the diamond is not changed significantly by increasing the temperature. The logarithmic plot of the Coulomb diamonds measured in the close vicinity of the charge neutrality point displays a rich excited state spectrum. We observe lines of increased conductance outside the diamonds running parallel to the diamond edges, which are well aligned to inelastic cotunneling onsets visible as faint horizontal (constant bias) structures inside the diamond-shaped regions (see arrows). At the diamond boundary, the horizontal lines seamlessly join some of the most prominent diagonal lines in the non-blockaded region, allowing to extract characteristic excitation energies in the range of 2 to 3 meV.

In addition, we observe for positive bias $V_b > 0$ V unconventional features inside the Coulomb-blockaded regions (see dashed lines) consisting of diagonal lines running parallel to the diamond edge. The fact that they have the same slope as the diamond edges suggests that they are connected to the alignment of an energy level with source (negative slope) or drain (positive slope). The vertical distance between the diagonal lines and the diamond edge is identical for lines with positive and negative slope (see dashed line inside the diamond). It has been shown by Schleser et al. [33] that these features are related to sequential tunneling through the quantum dot, occurring after it has been excited by an inelastic cotunneling process. In simple terms, these features can be attributed to a transport configuration where the tunneling-out rate from the excited state is significantly larger than the relaxation rate to the ground state, which might be directly related to strongly non-linear energy

dependences of the tunneling barriers. Finally, we also observe regions of negative differential conductance (see red areas), which are not yet fully understood.

Coulomb resonances as a function of a perpendicular magnetic field

In Fig. 3 we show more than 40 Coulomb resonances as a function of a B-field perpendicular to the graphene plane. The measurement has been taken in the back gate voltage range from $V_{bq} = -3.5$ to 6 V (also highlighted by the vertical line [B] in Fig. 1 and Fig. 1(e) in Ref. [8]). Thus we certainly tune from hole to electron transport (see arrows in Fig. 1). The evolution of Coulomb resonances in (perpendicular) magnetic field shows signatures of the electron-hole crossover of the quantum dot states (see below and Ref. [8]). There is a common trend of resonances at lower back gate voltages (see, e.g., resonances at $V_{bq} = 0$ V) to bend for increasing B-field towards higher energies (higher V_{bq}). In contrast we find for higher back gate voltage the opposite trend (see, e.g., resonances and arrow at $V_{bq} \approx 5.8 \text{ V}$), where resonances tend to shift to lower energies for increasing magnetic field. This overall pattern is disturbed by additional features such as localized states, regions of multi-dot behavior and strong amplitude modulations due to constriction resonances. For example, we observe a strongly elevated background below $V_{bq} < -1$ V, which can be attributed to the increase of the transparency of the tunneling barriers in agreement with the measurement presented in Fig. 1. Additionally, we observe between $V_{bq} = -1$ and 0 V a weakly coupled state crossing the Coulomb resonances at finite magnetic fields. We interpret the weak magnetic field dependence and low visibility in transport as a manifestation of a strongly localized state. Moreover, we see several level crossings and splittings in the region above $V_{bq} = 4$ V, which might be due to the presence of an additional quantum dot spontaneously forming in one of the two constrictions, and coupling to the gates with different lever arms [8].

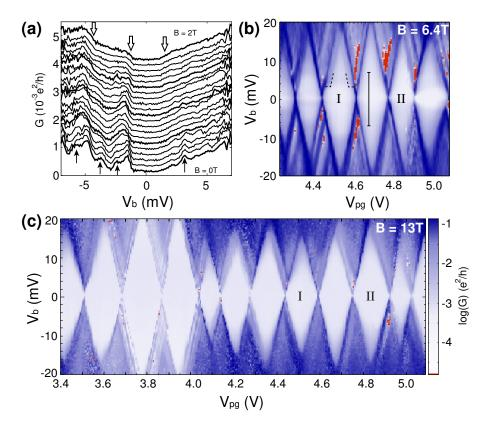


FIG. 4: (color online) (a) Evolution of inelastic cotunneling onsets inside the Coulomb-blockaded region in perpendicular magnetic field. The conductance is plotted as function of bias V_b and magnetic field B=0 to 2 T (stepped in units of 0.1 T) for constant plunger gate voltage $V_{pg}^*=4.66$ V [see vertical line in panel (b)]. For clarity the individual traces have been offset by $0.2 \times 10^{-3} e^2/h$. The peaks related to inelastic cotunneling marked by arrows quickly vanish as function of B. (b,c) Coulomb diamond measurements at B=6.4 T (b) and B=13 T (c), respectively. These measurements are taken at constant back gate voltage V_{bg} -0.9 V and highlight both (i) single dot signatures at high magnetic fields and (ii) the strong suppression of excited state-related signatures at higher B-fields.

Finally, in close analogy to Ref. [8] where the same sample was investigated in a different parameter regime we observe "kink" features with increasing B-field. It has been found that with increasing magnetic field the levels feature a kink signifying filling factor $\nu = 2$ in the dot (see dashed lines and arrows in Fig. 3) before converging toward the E=0 Landau level, in analogy to what has been observed in GaAs quantum dots [34]. In particular, the population of the lowest Landau level leads to a region around E = 0 [8, 32] with a remarkably ordered addition spectrum, which emerges for large magnetic fields (see also the analytical calculations for a circular dot [19, 20]). This feature is a unique consequence of the interplay of the unique Landau level spectrum in graphene [24, 25] and the carrier confinement due to the finite size of the system. For more details, including numerical simulations of graphene quantum dots and a quantitative discussion of the peak-to-peak spacing evolution in B-field we refer to Refs. [8, 32].

Coulomb diamonds at finite magnetic field

In Fig. 4a we show the evolution of inelastic cotunneling onsets inside the Coulomb-blockaded region as a function of perpendicular magnetic field. The conductance is plotted as a function of bias voltage V_b and magnetic field at constant plunger gate voltage $V_{pg} = 4.66 \text{ V}$ [see vertical line in Fig. 4(b)] and the B-field has been stepped by 0.1 T from B = 0 to 2 T. While at B = 0 T we observe several peaks and steps (black and white arrows), at B = 2 Tthe trace is smoother with remaining steps at 1.4 mV, -1.3 mV and 4.5 mV (white arrows). The different B-field dependence of the features might be attributed to two origins. The fine structures disappearing at B = 0.15 T(black arrows) may arise from energy dependent fluctuations of the barrier transmission, while the steps (white arrows) are attributed to the onset of inelastic cotunneling channels. This is supported by Figs. 4(b),(c), where we show Coulomb diamond measurements at B = 6.4 Tand B = 13 T. These measurements are taken at the same constant back gate voltage $V_{bg} = -0.9 \text{ V}$ as in Fig. 2(b)

and are plotted with the same colorscale. Thus, we can directly compare Figs. 2(b), 4(b) and 4(c) simplified by the diamond labels I and II [see Figs. 4(b),(c); the diamond shown in Fig. 2(b) corresponds to diamond II]. The horizontal (constant bias) lines in the Coulomb blockaded region present at B = 0 T are absent at higher B-fields. However, at B = 6.4 T cotunneling onsets and the unconventional feature consisting of diagonal lines inside the diamond [see above and dashed lines in Fig. 4(b)] can still be observed, but in a different diamond than at B = 0 T (I instead of II). At B = 13 T all excited-state related signatures inside the diamond are suppressed. In addition, also the negative differential conductance outside the diamond is significantly reduced and might also be related to a decrease in the energy dependent fluctuation of the barrier transmission. However, from these measurements we can conclude that the single-dot behavior of this etched graphene quantum dot device stays well preserved also for high magnetic fields.

CONCLUSION

We have performed detailed studies of transport through a graphene quantum dot in the vicinity of the charge neutrality point. The evolution of Coulomb resonances in magnetic field showed signatures of Landau level formation. Indications for the crossing of filling factor $\nu = 2$ are obtained by the observation of "kinks" in spectral lines before bending towards the charge neutrality point. Coulomb blockade diamonds at B=0 T near the electron-hole crossover show many excited states and cotunneling onsets accompanied by diagonal lines in the diamond attributed to cotunneling mediated sequential tunneling through an excited state. Many small scale lines inside the diamond disappear quickly (B = 1.5 T)in a magnetic field while more step like features (cotunneling onsets) are still visible at $B = 6.4 \,\mathrm{T}$. The presented measurements open the way for an in-depth exploration of the few charge carrier regime including addition spectra in graphene quantum dots.

The authors wish to thank F. Libisch, J. Seif, P. Studerus, C. Barengo, T. Helbling and S. Schnez for help and discussions. Support by the ETH FIRST Lab, the Swiss National Science Foundation and NCCR nanoscience are gratefully acknowledged.

- [1] M. Y. Han, B. Özyilmaz, Y. Zhang, and P. Kim, Phys. Rev. Lett., 98, 206805 (2007)
- [2] Z. Chen, Y.-M. Lin, M. Rooks and P. Avouris, Physica E, 40, 228, (2007)
- [3] X. Li, X. Wang, L. Zhang, S. Lee, H. Dai, Science, 319, 1229 (2008)

- [4] (i) C. Stampfer, J. Güttinger, F. Molitor, D. Graf, T. Ihn, and K. Ensslin, Appl. Phys. Lett., 92, 012102 (2008), (ii)
 C. Stampfer, E. Schurtenberger, F. Molitor, J. Güttinger, T. Ihn, and K. Ensslin, Nano Lett., 8, 2378 (2008)
- [5] L. A. Ponomarenko, F. Schedin, M. I. Katsnelson, R. Yang, E. H. Hill, K. S. Novoselov, A. K. Geim, Science, 320, 356 (2008)
- [6] J. Güttinger, C. Stampfer, S. Hellmüller, F. Molitor, T. Ihn, and K. Ensslin, Appl. Phys. Lett., 93, 212102 (2008)
- [7] S. Schnez, F. Molitor, C. Stampfer, J. Güttinger, I. Shorubalko, T. Ihn, and K. Ensslin, Appl. Phys. Lett., 94, 012107 (2009)
- [8] J. Güttinger, C. Stampfer, F. Libisch, T. Frey, J. Burgdörfer, T. Ihn, and K. Ensslin, submitted, arXiv:0904.3506 (2009)
- [9] K. Todd et al., Nano Lett. 9, 416 (2009)
- [10] X. Liu et al., arXiv:0812.4038 (2009)
- [11] K. A. Ritter and J. W. Lyding, Nat. Mater., 8, 235 (2009)
- [12] A. K. Geim and K. S. Novoselov, Nat. Mater., 6, 183 (2007)
- [13] M. I. Katnelson, Materials Today, 10(1-2), 20 (2007)
- [14] B. Trauzettel, D. V. Bulaev, D. Loss, and G. Burkard, Nature Physics, 3, 192, (2007)
- [15] C. L. Kane and E. J. Mele, Phys. Rev. Lett., 95 (2005)
- [16] H. Min et al., Phys. Rev. B, 74, 165310 (2006)
- [17] D. Huertas-Hernando, F. Guinea, and A. Brataas, Phys. Rev. B, 74, 155426 (2006)
- [18] M. V. Berry and R. J. Mondragon, Proceedings of the Royal Society of London, A, 412, 53-74 (1987)
- [19] S. Schnez, K. Ensslin, M. Sigrist, and T. Ihn, Phys. Rev. B, 78, 195427 (2008)
- [20] P. Recher, J. Nilsson, G. Burkard, and B. Trauzettel, Phys. Rev. B, 79, 085407 (2009)
- [21] F. Libisch, C. Stampfer, and J. Burgdörfer, Phys. Rev. B. 79, 115423 (2009)
- [22] A. F. Young and P. Kim, Nature Phys., 5, 222-226 (2009)
- [23] For review see, e.g., A. H. Castro Neto, F. Guinea, N. M. Peres, and A. K. Geim, Rev. Mod. Phys. 81, 109 (2009)
- [24] K. S. Novoselov, A. K. Geim, S. V. Morozov, D. Jiang, M. I. Katsnelson, I. V. Grigorieva, S. V. Dubonos, A. A. Firsov, Nature, 438, 197-200, (2005).
- [25] Y. Zhang, Y.-W. Tan, H. L. Stormer, P. Kim, Nature, 438, 201-204, (2005).
- [26] N. Dombay, and A. Calogeracos, Phys. Rep., 315, 4158 (1999)
- [27] M. I. Katsnelson, K. S. Novoselov, and A. K. Geim, Nature Phys. 2, 620625 (2006)
- [28] K. S. Novoselov, A. K. Geim, S. V. Morozov, D. Jiang, M. I. Katsnelson, S. V. Dubonos, I. V. Grigorieva, A. A. Firsov, Science, 306, 666, (2004).
- [29] F. Molitor, J. Güttinger, C. Stampfer, D. Graf, T. Ihn, and K. Ensslin, Phys. Rev. B 76, 245426 (2007).
- [30] C. Stampfer, J. Güttinger, S. Hellmüller, F. Molitor, K. Ensslin, and T. Ihn, Phys. Rev. Lett., 102, 056403 (2009)
- [31] F. Molitor, A. Jacobsen, C. Stampfer, J. Güttinger, T. Ihn, and K. Ensslin, Phys. Rev. B, 79, 075426 (2009)
- [32] F. Libisch et al., to be published.
- [33] R. Schleser, T. Ihn, E. Ruh, K. Ensslin, M. Tews, D. Pfannkuche, D. C. Driscoll, and A. C. Gossard, Phys. Rev. Lett., 94, 206805 (2005)
- [34] M. Ciorga, A. S. Sachrajda, P. Hawrylak, C. Gould, P. Zawadzki, S. Jullian, Y. Feng, and Z. Wasilewski, 2000, Phys. Rev. B, 61, R16315 (2000)